AIP | Review of Scientific Instruments

# Prediction of atomic force microscope probe dynamics through the receptance coupling method

M. Mehrpouya and S. S. Park

Citation: Review of Scientific Instruments **82**, 125001 (2011); doi: 10.1063/1.3664787
View online: http://dx.doi.org/10.1063/1.3664787
View Table of Contents: http://scitation.aip.org/content/aip/journal/rsi/82/12?ver=pdfcov
Published by the AIP Publishing

**Articles you may be interested in**

Note: Seesaw actuation of atomic force microscope probes for improved imaging bandwidth and displacement range
Rev. Sci. Instrum. **82**, 086104 (2011); 10.1063/1.3622748

Lateral force measurement using a probe fiber as a microlens
J. Appl. Phys. **95**, 5189 (2004); 10.1063/1.1691479

Scanning Hall probe microscopy on an atomic force microscope tip
J. Vac. Sci. Technol. A **19**, 1769 (2001); 10.1116/1.1379324

Force based displacement measurement in micromechanical devices
Appl. Phys. Lett. **78**, 4031 (2001); 10.1063/1.1380398

Monitoring of an atomic force microscope cantilever with a compact disk pickup
Rev. Sci. Instrum. **70**, 3620 (1999); 10.1063/1.1149969


This article is copyrighted as indicated in the article. Reuse of AIP content is subject to the terms at: http://scitationnew.aip.org/termsconditions. Downloaded to IP: 35.8.11.3 On: Mon, 25 Jan 2016 01:52:26

# Prediction of atomic force microscope probe dynamics through the receptance coupling method

M. Mehrpouya and S. S. Park[a)]
*Micro Engineering, Dynamics and Automation Laboratory (MEDAL), Department of Mechanical and Manufacturing Engineering, University of Calgary, Calgary, Alberta T2N 1N4, Canada*

(Received 28 July 2011; accepted 6 November 2011; published online 7 December 2011)

The increased growth in the use of tip-based sensing, manipulations, and fabrication of devices in atomic force microscopy (AFM) necessitates the accurate prediction of the dynamic behavior of the AFM probe. The chip holder, to which the micro-sensing device is attached, and the rest of the AFM system can affect the overall dynamics of the probe. In order to consider these boundary effects, we propose a novel receptance coupling method to mathematically combine the dynamics of the AFM setup and probe, based on the equilibrium and compatibility conditions at the joint. Once the frequency response functions of displacement over force at the tool tip are obtained, the dynamic interaction forces between the tip and the sample in nanoscale can be determined by measuring the probe tip displacement. © *2011 American Institute of Physics*. [doi:10.1063/1.3664787]

## I. INTRODUCTION

In recent years, the demand for microscale and nanoscale instruments has increased the need for characterization and fabrication of micro- and nano-sized structures. An atomic force microscope is an important tool in nanotechnology with its unmatched capabilities of measuring topography, nanoscale fabrications, and characterizing the properties of various materials.

Atomic force microscopy (AFM) is a tip-based technology that measures interactions between a sharp tip and the atomic surface by determining the vibration of the tip through a laser system. During a surface scan in the non-contact mode, the probe is vibrated just above its natural frequency. As the probe scans over a surface, a constant force between the tip and the sample is maintained through a fast servo system; and, the movement of the scanner and the phase response of the probe provide the surface topography.

The tip-based method can also be used to fabricate nanoscale grooves and channels with a maximum depth of a few micrometers. Some of the applications of scribed nanogrooves using AFM probes include molds for liquid crystal backlight guides, channels in micro-fluidic devices, and maskless lithography. The characterization of mechanical scribing in the nanoscale based on AFM probes entails the determination of sensitivity factors, spring constants and lateral and vertical forces during scratching.[1]

Nano-scribing uses a nano-sized tip to make mechanical contact with the surface in order to create nanoscale features of a defined size, shape, and spatial position. The operational principle is much like that of traditional macroscale orthogonal cutting operations, where forces are applied to a probe to indent and plastically deform the workpiece material.[2] The relation between applied forces and the cutting dimensions is embedded in the dynamics of the probe at the cutting tip. Obtaining the exact cutting dimensions in the nanoscale requires accurate knowledge of the dynamics of the probe, in order to calculate the amount of force needed for a certain feature.

Moreover, many of the scanning processes are also sensitive to the dynamic characteristics at the tool tip. If such dynamic characteristics are identified incorrectly, inaccurate results from topographic scanning, vertical force measurements, and lateral force spectroscopy may be obtained. Therefore, accurate dynamic measurements (i.e., receptance) of the system at the tip of the AFM probe are very important.

The images taken from AFM are very dependent on the vibration of the cantilever near the surface. When the probe comes close to the surface, the tip oscillation is influenced by the interaction forces and both the amplitude and phase, the phase difference between the probe oscillation and the driving frequency, of the probe oscillation varies. The AFM feedback control system compensates for the changes in the vibration amplitude of the probe by moving the Z stage.

In particular, at a certain range of vibration amplitudes in dynamic AFM, there may exist two corresponding Z-stage distances from the surface in the feedback control loop.[3] The coexistence of two separation distances for a certain vibration amplitude may cause the Z stage to jump from one state to the other state with any changes in the topography of the sample; and, this movement can be interpreted as a change in the sample's topography. This phenomenon culminates in image instability, with the images usually getting contaminated with artifacts.[4,5]

These unstable ranges should be defined using amplitude-modulation curves (vibration amplitude versus Z-stage distance from the sample) before starting any scanning processes, so that reliable topography and phase images can be obtained. To produce amplitude-modulation curves, the exact dynamics of the probe at the tip and the interaction force model are needed. By having the exact behavior of the probe, the extended probe dynamics, with consideration of nonlinear interaction forces between the probe and the sample, can be employed in generating the amplitude-modulation curve.

a)Electronic mail: simon.park@ucalgary.ca.

 © 2011 American Institute of Physics

This article is copyrighted as indicated in the article. Reuse of AIP content is subject to the terms at: http://scitationnew.aip.org/termsconditions. Downloaded to IP: 35.8.11.3 On: Mon, 25 Jan 2016 01:52:26

With knowledge of the dynamics of the probe at the tip, good insight can be provided for any extension of AFM operational modes, such as atomic force acoustic microscopy (AFAM). In this operational mode, which is actually an extension of the contact mode, the probe tip is in contact with the sample and forms a contact mechanism based on the sample characteristic. An ultrasonic transducer excites the sample causing the whole mechanism to vibrate and reveal the contact mechanism's properties through amplitude and phase images.[6] When the exact probe dynamics up to the tip is available, it can be modified by adding the contact mechanism to study the probe movement under the excitation of the sample. Different contact mechanisms form different mechanical systems with unique vibrational properties. Therefore, the accurate measurement and prediction of the AFM probe's dynamics are imperative for a variety of applications.

Several researchers have investigated the analytical dynamics of the AFM probe.[7,8] Mendels *et al.*[9] provided a numerical finite element (FE) model and analytical Timoshenko beam model for the AFM probe and extracted the first ten natural frequencies and corresponding mode shapes. The obtained mode shapes were then optimized, based on the experimentally obtained modes, to improve the uncertain physical parameters of the probe. Melcher *et al.*[10] presented a point-mass system to model the continuous AFM cantilever beam for a general eigenmode of arbitrarily shaped AFM probes, based on the equivalence of kinetic and strain energies.

Salehi-Khojin *et al.*[11] provided a theoretical model for a nano-mechanical cantilever probe that considered the piezoelectric layer's dynamic effects in the model. They validated the proposed model with experimentally obtained natural frequencies and mode shapes and showed that a uniform model for the probe failed to precisely predict the actual behavior.

Arinero and Leveque[12] developed a FE model for contact mode AFM that took into account different beam shapes, sample stiffnesses and contact models and studied the slip and slide phenomenon at different driving frequencies and vibration amplitudes. When an AFM cantilever is brought near a sample in the non-contact mode, the tip-surface interaction forces greatly influence the cantilever dynamics.[13] If the dynamic behavior of the cantilever is about to be studied in the non-contact mode, the effects of these forces on the probe dynamics should also be investigated.

Hu *et al.*[14] used harmonic balance based nonlinear system identification methods to extract the forces between a few atoms of the tip and the sample, using the nonlinear vibration spectrum of resonant atomic force silicon microcantilevers. In the absence of electrostatic, hydration, and magnetic forces, they supposed that the only acting force on the tip would be the Van der Waals force, which has an inverse relationship with the tip-sample distance. Sasaki *et al.*[15] also investigated the cantilever dynamics in the non-contact mode, based on the point-mass equivalent model.

However, the existing methods, such as the FE methods, do not provide accurate receptance (i.e., displacement/force) measurements at the tip for a wide range of frequencies. The majority of studies that have been conducted on the dynamics of microprobes have neglected the importance of boundary conditions at the tool base and assumed a simple cantilever beam. This results in discrepancy between the analytical and actual dynamics, mainly due to the assumptions that were considered for the system modeling and boundary conditions.

Direct experimental modal analysis techniques using an instrumented hammer are also not applicable for the AFM probe, due to its fragility; therefore, a modified technique should be employed. Park *et al.*[16] and Schmitz[17] have investigated the receptance coupling (RC) technique, which mathematically couples analytically or experimentally obtained frequency response functions (FRFs) of the substructure components to predict the overall response of the assembled structure.

The objective of this study is the determination of the accurate receptances of the probe for wide frequency ranges. Most of the previous studies on the dynamics of AFM probe dismissed the effects of the joint between the probe and the holder setup. In this study, we attempt to investigate these effects by coupling the experimentally identified dynamics of the holder with the mathematical model of the probe. It is assumed that geometrical nonlinearities are avoided by applying low voltage to the base and that the cantilever dynamics is studied far from the surface to avoid nonlinear interaction effects between the probe and sample surface.

The direct FRFs of the probes are obtained at the tip end through the receptance coupling method by indirectly coupling the FE model of the free-free probe and the dynamics of the AFM system (i.e., boundary condition) obtained from measurements. With this method, we can obtain accurate dynamics of the probe at the tip, which can be used for non-contact material characterizations through phase[18] and AFAM. The dynamic forces in linear ranges can also be acquired to investigate the atomic tip-surface interactions during nanoscale fabrication process.

In this paper, we first discuss the experimental setup. The setup includes the AFM and cantilever systems, including a chip containing three tipless probes. The calibration procedure, which is required to acquire the necessary sensitivity factors, is also discussed. An extended receptance coupling method is then proposed to obtain the overall assembled dynamics at the tool tip. In this method, we first use the information obtained from two tipless beams to extract the dynamics of the holder system and then use measurements on the third tipless probe as verification of the obtained dynamics. Moreover, the probe system is replaced with a conventional probe that contains a tip, in order to verify the effectiveness of the obtained information for the holder setup on other probes.

## II. EXPERIMENTAL SETUP

A retrofitted commercial atomic force microscope (Park Systems XE-100), as shown in Figure 1, was used in the experiments. The flexure-based piezoelectric XY stage of the AFM system provided accurate motions with an independent Z stage. The AFM laser setup allowed for the monitoring of the movement of the Z stage. The probe deflection was measured using a laser and a position sensitive photodiode (PSPD). Data acquisition systems (Park AFM Signal Access Module, NI BNC-2110, and NI PCI 6251) facilitated the capture of the necessary signals at high-frequency sampling rates.

This article is copyrighted as indicated in the article. Reuse of AIP content is subject to the terms at: http://scitationnew.aip.org/termsconditions. Downloaded to IP: 35.8.11.3 On: Mon, 25 Jan 2016 01:52:26

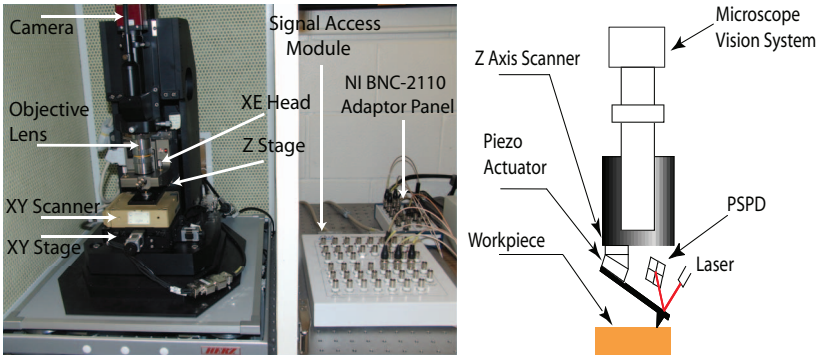


FIG. 1. (Color online) (a) AFM setup; (b) schematics of the setup.

In addition, the signals were filtered through anti-aliasing filters (Krohn Hite 3364) with the cut-off frequency equal to the half of the sampling frequency.

The probes that were used in this study contained three tipless cantilever beams (MikroMasch CSC12) made of silicon ($\rho = 2330$ kg/m$^3$, E = 112 GPa) with a nominal width of 35 $\mu$m, thickness of 1.0 $\pm$ 0.3 $\mu$m and lengths of 350, 250, and 300 $\mu$m for probes A, B, and C, respectively. The other cantilever, which was used in the verification section, was a MikroMasch CSC38 aluminum-coated silicon probe. The probe was comprised of a rectangular beam made of silicon ($\rho = 2330$ kg/m$^3$, E = 112 GPa) with a nominal width of 35 $\mu$m, thickness of 1.0 $\pm$ 0.3 $\mu$m and length of 350 $\mu$m. A tetrahedron-shaped silicon tip with a height of approximately 20 $\mu$m and a tip cone angle of 40° was also pointed close to the free end of the probe. The mass for the tip part, which was approximately $4.03 \times 10^{-12}$ kg, was calculated by multiplying the volume of the tetrahedron tip section ($\sqrt{12}/16$ h$^3$) and the density of silicon (2330 kg/m$^3$).

The sensitivity of the PSPD in the AFM setup is vital to ensuring the accuracy of the measured data. The vertical voltage on the PSPD was measured independently as $V_N$ ('A-B' of PSPD). To convert this voltage signal into units of vertical displacement, it must be multiplied by a calibration constant, $S_N$. This constant was found using force-displacement (FD) curves, which were obtained by bringing the probe down onto a hard surface, such as a diamond surface. The sensitivity ($\mu$m/V) was obtained by taking the inverse slope of the FD curve as

$$S_N = \frac{\delta_{cantilever}}{\Delta V}, \tag{1}$$

where $\delta_{cantilever}$ is the cantilever deflection and $\Delta V$ is the difference in the output voltage from the PSPD. The FD curve compensates for the hysteresis of the piezo actuator. The normal sensitivity factors, $S_N$, for the different cantilevers are presented in Table I.

TABLE I. Vertical sensitivities.

| Probe | A | B | C | CSC38 |
|---|---|---|---|---|
| Sensitivity, $S_N$ ($\mu$m/V) | 0.0248 | 0.0235 | 0.0549 | 0.0487 |

The AFM setup included a piezoelectric bimorph actuator to mechanically vibrate the cantilever (Figure 2). The piezo modulator, which was mounted beneath the Z stage, was actuated by a chirp voltage signal in this study; and, the response of each cantilever was detected using a laser and a quad PSPD. The chirp signal covered the frequency range of 0–600 kHz, which was generated for 3 s, and included the dominant natural frequencies of the cantilevers used in this study.

A spectral analysis[19] was then performed to obtain the FRFs for individual beams. To obtain the FRFs for the cantilevers, it was assumed that the excitation from the piezo stack was transferred to the base of the probe (Figure 2). Therefore, the whole setup was modeled as an equivalent mass ($m_{eq}$), representing the probe (and tip) mass, an equivalent spring ($k_{eq}$), representing the probe stiffness, and a moving base, representing the movement transferred to the base of the probe ($x_2$).[10] Therefore, the equation of motion for this system can then be written as

$$m_{eq}\ddot{x}_1 + k_{eq}x_1 = F_2 \approx k_{eq}x_2, \tag{2}$$

where $x_1$ is the movement of the probe tip. This implies that the applied force from the piezo actuator to the cantilever is $k_{eq}x_2$. The FRF is then the movement of the probe tip divided by the applied force in the frequency domain.

To obtain these FRFs, the following procedure was employed. First, each cantilever was excited with a chirp signal that contained a frequency content of up to 600 kHz. The measurements were done on the tip of each probe while the laser was shining at the tip. The recorded values were considered as the response of probe at the tip to the chirp excitation. The laser was then directed on the base of the probes, and the response to the same chirp signal at that point was recorded.

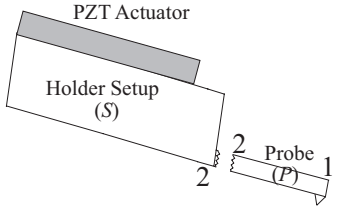


FIG. 2. Probe holder substructure setup.

This article is copyrighted as indicated in the article. Reuse of AIP content is subject to the terms at: http://scitationnew.aip.org/termsconditions. Downloaded to IP: 35.8.11.3 On: Mon, 25 Jan 2016 01:52:26

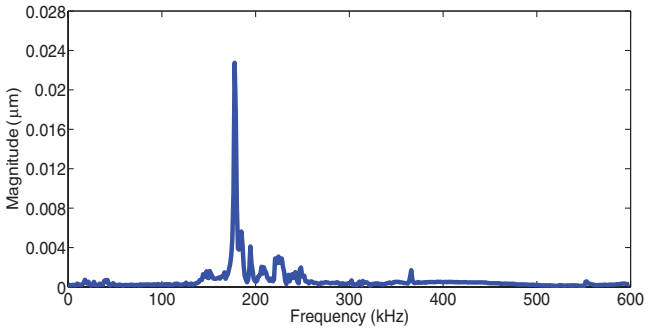


FIG. 3. (Color online) Frequency content of the recorded displacement at the base for probe A.

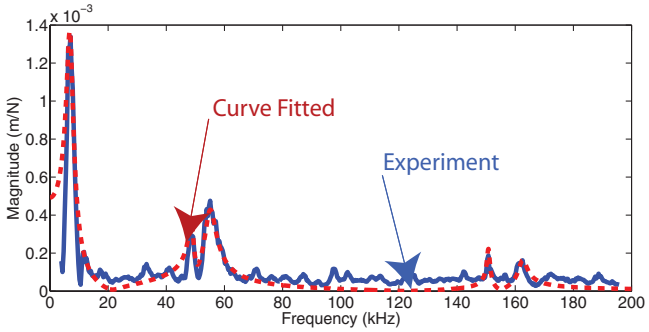


FIG. 4. (Color online) Frequency response function of probe A ($G_{12,ff}$).

Using Eq. (3), the FRF for each probe was obtained as

$$G_{12}(\omega) = \frac{x_1}{F_2} \approx \frac{x_1(\omega)}{k_{eq} x_2(\omega)}, \tag{3}$$

where $x_1$ and $x_2$ are the frequency contents of the recorded response at the probe tip and the base of the probe, respectively.

In this study, it was assumed that the equivalent stiffness was equal to the static stiffness of the probe provided by the vendor. The frequency content of the recorded displacement at the base of probe A in response to the 1 V chirp excitation is shown in Figure 3, as an example. The displacement values were obtained by multiplying the recorded voltage from the PSPD with the sensitivity of the probe (0.0248 $\mu$m/V).

When the FRF curves were obtained for each probe, the damping coefficients for the beams could be obtained through the curve-fitting method.[20] We used a simple single degree of freedom (SDOF) approach, called the peak-picking method, which assumed that the response could be attributed to the local mode and the contribution of other modes could be ignored. First, individual resonance peaks ($\omega_{n,r}$) and their corresponding FRF value (|H|) were detected from the FRF curve. Then, two frequencies on each side of the natural frequency, called half-power points, were chosen. These two points ($\omega_a$ and $\omega_b$) were located at the response level equal to $|H|/\sqrt{2}$.

The damping ratios were then defined as in Eq. (4a). The modal constant was also obtained from the identified damping ratio, the natural frequency, and the response amplitude at the corresponding natural frequency, as in Eq. (4b). The formulation used for the curve fitting after obtaining the modal parameters is presented in Eq. (4c).

$$\zeta_r = \frac{\omega_a^2 - \omega_b^2}{4\omega_r^2}, \tag{4a}$$

$$_rA_{ij} = 2|H_{ij}|\omega_r^2 \zeta_r, \tag{4b}$$

$$G_{ij}(\omega) = \sum_{r=1}^{N} \frac{_rA_{ij}}{\omega_{n,r}^2 - \omega^2 + 2j\zeta_r \omega_{n,r}\omega}, \tag{4c}$$

where $A_{ij}$ is the modal constant, $\omega_n$ is the natural frequency, and $\zeta_r$ is the damping ratio at each natural frequency.

Figure 4 shows the FRF of probe A and the fitted curve over the FRF using Eq. (4c). Subscript $f$ represents the translational degree of freedom (DOF) and $m$ represents the rotational DOF of the probe. For instance, $G_{12,ff}$ means the FRF obtained from the measured translational movement of point 1 in Figure 2 when the translational force is applied at point 2. Since rotational FRFs also make a significant contribution to the dynamics of the probe, both rotational and translational FRFs were considered in this study. The natural frequencies and their corresponding damping ratios for different probes are presented in Table II.

The procedure described for identifying the FRFs and modal parameters was employed for all three tipless probes and the CSC38 probe. The FRFs for each probe were obtained when the force was applied at point 2, and two separate measurements were done, at point 1 ($x_1$) and point 2 ($x_2$) in Figure 2. The importance of having FRFs for each probe is their significance in the determination of the applied forces to the probe when the displacement data are measured.

The FRFs and information obtained from the curve fitting method were then used in the RC procedure, which enabled us to obtain the direct point FRF at the tool tip and also the dynamics of the holder setup up to the probe base. The dynamics of the holder setup was of interest, because it can be considered as an inherent property of the AFM setup and can be coupled with the mathematical model of any probe whenever a new probe is installed, in order to obtain the exact dynamics at the probe tip.

## III. METHODOLOGY AND RESULTS

### A. Receptance coupling

The RC method, in essence, is the mathematical combination of the FRFs of the subcomponents, obtained analytically or experimentally, based on the compatibility and equilibrium conditions at the joint parts.[16,17,21,22] Using the RC method, it is possible to obtain the assembled dynamics based on the substructures' information. Consider that we have

TABLE II. Natural frequencies and damping ratios.

| Probe | A | B | C | CSC38 |
|---|---|---|---|---|
| $\omega_{n,1}$ (kHz) | 7.03 | 12.80 | 10.94 | 9.6 |
| $\zeta_1$ | 0.1667 | 0.0787 | 0.1227 | 0.1667 |
| $\omega_{n,2}$ (kHz) | 48.8 | 78.5 | 74.61 | 18.0 |
| $\zeta_2$ | 0.0199 | 0.0086 | 0.0157 | 0.0199 |
| $\omega_{n,3}$ (kHz) | 55.08 | 150.4 | 150.8 | 42.0 |
| $\zeta_3$ | 0.0354 | 0.004 | 0.0030 | 0.0354 |

This article is copyrighted as indicated in the article. Reuse of AIP content is subject to the terms at: http://scitationnew.aip.org/termsconditions. Downloaded to IP: 35.8.11.3 On: Mon, 25 Jan 2016 01:52:26

information regarding substructure $P$ from the FE model and information of substructure $S$ from experiments (Figure 5). Through the RC method, it is viable to obtain the assembled dynamics based on the information of these two substructures without any necessity for performing experiments on the assembled structure. In the formulations, symbol $G$ represents the dynamics of the assembly, while $H$ represents the dynamics of substructures.

We employed inverse RC methodology on the AFM probe application to extract the necessary information about the holder dynamics, which was of interest in this study. Substructure $S$ in this application represented the AFM holder setup, which was coupled with the free-free FE model of the probe. Since we had information about the assembly dynamics and also the FE model of the probe, the holder dynamics could be extracted using the inverse procedure of RC. Figure 2 considers the case where the whole structure was divided into two substructures: the holder ($S$) and the probe ($P$). The structural dynamic model (i.e., FRF) of the probe (substructure $P$) could be obtained using either the beam theory or an FE method

$$\begin{Bmatrix} X_1 \\ X_{P,2} \end{Bmatrix} = \begin{bmatrix} H_{P,11} & H_{P,12} \\ H_{P,21} & H_{P,22} \end{bmatrix} \begin{Bmatrix} F_1 \\ F_{P,2} \end{Bmatrix}, \tag{5}$$

where $X$ and $F$ are the displacement and force vectors applied on the probe at points 1 and 2 in Figure 2, and $H_{P,ij}$ are the FRFs between points $i$ and $j$. Similarly, the FRF of the holder structure ($S$) at its free end (point 2) is

$$\{X_{S,2}\} = [H_{S,22}]\{F_{S,2}\}. \tag{6}$$

The equilibrium and compatibility conditions at the probe-holder joint (point 2 in Figure 2) provide the following:

$$\begin{aligned} F_2 &= F_{S,2} + F_{P,2} \\ X_2 &= X_{S,2} = X_{P,2}. \end{aligned} \tag{7}$$

By substituting the compatibility and equilibrium conditions of Eq. (7) in the FRFs of Eqs. (5) and (6), the following equation is obtained:

$$\begin{aligned} X_2 &= H_{S,22}F_{S,2} = H_{P,21}F_1 + H_{P,22}F_{P,2}, \\ F_{S,2} &= (H_{P,22} + H_{S,22})^{-1}(H_{P,21}F_1 + H_{P,22}F_2). \end{aligned} \tag{8}$$

Letting $H_2 = (H_{P,22} + H_{S,22})$, displacements $X_1$ and $X_2$ can be expressed as functions of FRFs and applied forces $F_1$ and $F_2$ as follows:

$$\begin{aligned} X_1 &= H_{P,11}F_1 + H_{P,12}(F_2 - F_{S,2}) \\ &= H_{P,11}F_1 + H_{P,12}F_2 - H_{P,12}F_{S,2} \\ &= H_{P,11}F_1 + H_{P,12}F_2 - H_{P,12}H_2^{-1} \\ &\quad \times (H_{P,21}F_1 + H_{P,22}F_2) \\ &= (H_{P,11} - H_{P,12}H_2^{-1}H_{P,21})F_1 \\ &\quad + (H_{P,12} - H_{P,12}H_2^{-1}H_{P,22})F_2, \end{aligned} \tag{9}$$

$$\begin{aligned} X_2 &= H_{P,21}F_1 + H_{P,22}(F_2 - F_{S,2}) \\ &= H_{P,21}F_1 + H_{P,22}F_2 - H_{P,22}H_2^{-1}(H_{P,21}F_1 + H_{P,22}F_2) \\ &= \left(H_{P,21} - H_{P,22}H_2^{-1}H_{P,21}\right)F_1 + \left(H_{P,22} - H_{P,22}H_2^{-1}H_{P,22}\right)F_2. \end{aligned} \tag{10}$$

The equations can be rearranged in a matrix form as

$$\begin{Bmatrix} X_1 \\ X_2 \end{Bmatrix} = \begin{bmatrix} \left(H_{P,11} - H_{P,12}H_2^{-1}H_{P,21}\right) & \left(H_{P,12} - H_{P,12}H_2^{-1}H_{P,22}\right) \\ \left(H_{P,21} - H_{P,22}H_2^{-1}H_{P,21}\right) & \left(H_{P,22} - H_{P,22}H_2^{-1}H_{P,22}\right) \end{bmatrix} \begin{Bmatrix} F_1 \\ F_2 \end{Bmatrix}. \tag{11}$$

Equation (11) implies that, by having the FRFs of the substructures, the dynamics of the assembled structure can be extracted at the tip of probe, in response to forces acting at the same point ($G_{11} = X_1/F_1$) or in response to the forces acting on the holder ($G_{12} = X_1/F_2$). By extending Eq. (11), the assembled tool tip dynamics can be formulated as

$$\begin{aligned} \begin{bmatrix} G_{12,ff} & G_{12,fm} \\ G_{12,mf} & G_{12,mm} \end{bmatrix} &= \begin{bmatrix} H_{P12,ff} & H_{P12,fm} \\ H_{P12,mf} & H_{P12,mm} \end{bmatrix} - \begin{bmatrix} H_{P12,ff} & H_{P12,fm} \\ H_{P12,mf} & H_{P12,mm} \end{bmatrix} \left( \begin{bmatrix} H_{P22,ff} & H_{P22,fm} \\ H_{P22,mf} & H_{P22,mm} \end{bmatrix} \right. \\ &\quad \left. + \begin{bmatrix} H_{S22,ff} & H_{S22,fm} \\ H_{S22,mf} & H_{S22,mm} \end{bmatrix} \right)^{-1} \begin{bmatrix} H_{P22,ff} & H_{P22,fm} \\ H_{P22,mf} & H_{P22,mm} \end{bmatrix}. \end{aligned} \tag{12}$$

The first term of the assembled structure FRF ($G_{12,ff} = x_1/f_2$) is measured experimentally when the system undergoes the chirp excitation. $H_{P,12}$ and $H_{P,22}$ are the probe's receptance matrices found through the FE analysis. $H_{S,22}$ is the FRF of the holder setup at the base of the probe.

By considering the equality of the transverse FRF between the force and the momentum ($H_{S22,fm} = H_{S22,mf}$

This article is copyrighted as indicated in the article. Reuse of AIP content is subject to the terms at: http://scitationnew.aip.org/termsconditions. Downloaded to IP: 35.8.11.3 On: Mon, 25 Jan 2016 01:52:26

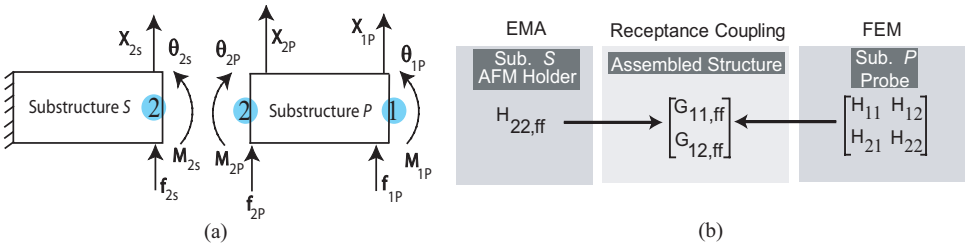


FIG. 5. (Color online) (a) Substructures in the uncoupled state, (b) RC procedure to couple substructures dynamics.

$= x_2/M_2$) and neglecting the small value of $H_{S22,mm} = \theta_2/M_2$, the number of unknown parameters is reduced to two ($H_{S22,mf}$ and $H_{S22,ff}$). It is possible to apply the same procedure on two probes (B and C) to form two equations. Solving the two equations simultaneously for the two unknowns, the holder dynamics ($H_{S22,mf}$, $H_{S22,ff}$) is identified as follows:

$$G_{12,ff} = \frac{x_1}{f_2}$$

$$= H_{P12,ff} + \left[H_{2,mf}^2 - H_{2,mm}H_{2,ff}\right]^{-1} \times [H_{P22,mf}(-H_{2,mf}H_{P12,ff} + H_{P12,fm}H_{2,ff}) + H_{P22,ff}(-H_{2,mf}H_{P12,fm} + H_{2,mm}H_{P12,ff})], \tag{13}$$

where $H_2$ represents the summation of $H_P$ and $H_S$ components, (i.e., $H_{2,ij} = H_{P22,ij} + H_{S22,ij}$). This equation can be rewritten as

$$v = b + \frac{g(-b(g + H_{S22,mf}) + e(d + H_{S22,ff})) + d(-e(g + H_{S22,mf}) + ab)}{(g + H_{S22,mf})^2 - a(d + H_{S22,ff})}, \tag{14}$$

where $G_{12,ff} = v$, $H_{P12,ff} = b$, $H_{P22,ff} = d$, $H_{P12,fm} = e$, $H_{P22,mf} = g$, $H_{P22,mm} = a$.

Rearranging Eq. (14) based on the two unknowns, $H_{S22,mf}$ and $H_{S22,ff}$, and applying the equations to two probes (B and C), we get

$$\begin{aligned}
&(v_B - b_B)\,H_{S22,mf}^2 + (2g_B v_B - g_B b_B + d_B e_B)\,H_{S22,mf} + (b_B a_B - a_B v_B - g_B e_B)\,H_{S22,ff} + \left(v_B g_B^2 - a_B d_B v_B\right) = 0,\\
&(v_C - b_C)\,H_{S22,mf}^2 + (2g_C v_C - g_C b_C + d_C e_C)\,H_{S22,mf} + (b_C a_C - a_C v_C - g_C e_C)\,H_{S22,ff} + \left(v_C g_C^2 - a_C d_C v_C\right) = 0.
\end{aligned} \tag{15}$$

Solving the two equations for the two unknowns leads to

$$H_{S22,mf} = \frac{-\left(n_1 - \frac{p_1}{p_2}n_2\right) \pm \sqrt{\left(n_1 - \frac{p_1}{p_2}n_2\right)^2 - 4\left(m_1 - \frac{p_1}{p_2}m_2\right)\left(q_1 - \frac{p_1}{p_2}q_2\right)}}{2\left(m_1 - \frac{p_1}{p_2}m_2\right)} \tag{16}$$

and

$$H_{S22,ff} = -\frac{m_2}{p_2}H_{S22,mf}^2 - \frac{n_2}{p_2}H_{S22,mf} - \frac{q_2}{p_2}, \tag{17}$$

where

$$\begin{aligned}
&m_1 = (v_B - b_B),\ m_2 = (v_C - b_C),\\
&n_1 = (2g_B v_B - g_B b_B + d_B e_B),\\
&n_2 = (2g_C v_C - g_C b_C + d_C e_C),\\
&p_1 = (b_B a_B - a_B v_B - g_B e_B),\ p_2 = (b_C a_C - a_C v_C - g_C e_C),\\
&q_1 = \left(v_B g_B^2 - a_B d_B v_B\right),\ q_2 = \left(v_C g_C^2 - a_C d_C v_C\right),
\end{aligned}$$

and subscripts B and C denote the parameters from probe B (i.e., length of 250 $\mu$m) and probe C (i.e., length of 300 $\mu$m), respectively.

Once the dynamic properties of the holder setup are defined, we are able to use them in the prediction of the direct FRF at the tip of probe. These FRFs can be employed in defining the vertical and torsional displacement of the tip, in response to the applied forces in the linear domain

$$\begin{bmatrix} G_{11,ff} & G_{11,fm} \\ G_{11,mf} & G_{11,mm} \end{bmatrix} = \begin{bmatrix} H_{P11,ff} & H_{P11,fm} \\ H_{P11,mf} & H_{P11,mm} \end{bmatrix} - \begin{bmatrix} H_{P12,ff} & H_{P12,fm} \\ H_{P12,mf} & H_{P12,mm} \end{bmatrix} \times \left( \begin{bmatrix} H_{P22,ff} & H_{P22,fm} \\ H_{P22,mf} & H_{P22,mm} \end{bmatrix} + \begin{bmatrix} H_{S22,ff} & H_{S22,fm} \\ H_{S22,mf} & H_{S22,mm} \end{bmatrix} \right)^{-1} \begin{bmatrix} H_{P21,ff} & H_{P21,fm} \\ H_{P21,mf} & H_{P21,mm} \end{bmatrix}. \tag{18}$$

This article is copyrighted as indicated in the article. Reuse of AIP content is subject to the terms at: http://scitationnew.aip.org/termsconditions. Downloaded to IP: 35.8.11.3 On: Mon, 25 Jan 2016 01:52:26

In formulating the problem, it was assumed that the receptance matrices were invertible. This assumption was verified by monitoring the condition number of the inverted matrices during the computations. Monitoring condition number is important, especially at high frequencies, where the condition number of some matrices may increase and measurement noise may result in inaccuracy of the obtained results. Rotational FRFs ($H_{S22,mm}$) were assumed to be negligible. This was verified through a FE simulation where the elimination of the rotational FRFs did not result in considerable deviation from the original results. Moreover, a system can behave with the non-minimum phase characteristics in a specific frequency range. In this case, the location of the transfer function non-minimum phase zeros is sensitive to errors. Therefore, the accuracy of the computations is limited by the minimum-phase frequency region of the system transfer functions.[23]

The prediction of the direct FRFs at the tool tip is important, since they can be used in the identification of the applied forces or displacement of the tool tip once one of these values is known. When the applied forces or displacements of the tip are defined, the area with excessive force or displacement, in which the probes become vulnerable, can be avoided. Thus far, the procedure to extract the holder dynamics and the FRFs at the probe tip has been introduced. The holder dynamics is an inherent property of the AFM setup, which does not change significantly when different chip setups are placed on the AFM holder head. When this property is identified once, it can be saved as invariable dynamics and can be used in further calculation without any need to repeat the experiments.

These procedures were employed on the experimental measurements performed on the different probes to identify the necessary information regarding the holder dynamics and then to validate the accuracy of the identified holder dynamics.

## IV. RESULTS AND DISCUSSIONS

We utilized the holder setup identification procedure on the tests that were conducted on the tipless probes. Using two sets of measurements on two different probes, the dynamics of the holder setup was identified, which was then used in two verification sets on the third tipless probe and the CSC38 probe. The FRFs for these two probes were predicted using the pre-identified holder dynamics and the RC method and were then compared with the directly measured FRFs from the experiments.

### A. Identification of the joint

Two sets of measurements on probes B and C were conducted to extract the FRF of $G_{12,ff}$ for each probe ($v_B$ and $v_C$ in Eq. (15)). These FRFs were obtained when the chirp signal was applied to the piezo stack and the measurements were done at point 1 in Figure 2. Constituting Eq. (14) for these two probes and solving the two equations for two unknowns ($H_{S22,mf}$ and $H_{S22,ff}$), the holder dynamics were extracted as presented in Eqs. (16) and (17).

The probe properties were obtained from the FE model using Euler-Bernoulli beam elements and a free-free boundary condition. Each beam was divided into 10 elements, and the damping ratios were extracted from Table II. Figures 6 and 7 show the direct FRFs of the translational vibration ($H_{S22,ff}$) and the rotational vibration ($H_{S22,mf}$) at the holder tip, respectively. In order to smooth out the undesirable noise effects from the original signal, the Savitzky-Golay filter[24] was applied to the results.

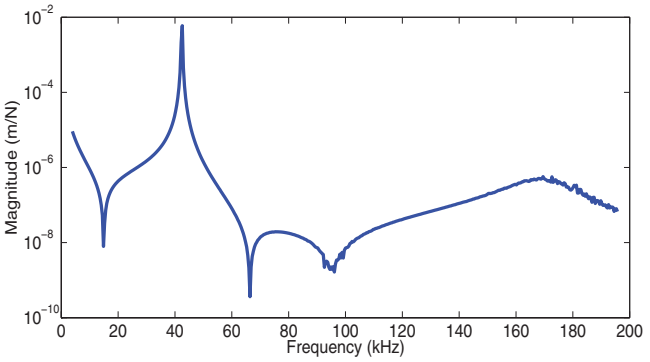


FIG. 6. (Color online) Translational FRF at the joint ($H_{S22,ff}$).

As shown in Figures 6 and 7, the holder setup had two dominant modes up to 200 kHz. Once the holder dynamics is available, it can be saved as an embedded property of the AFM setup that would not change considerably when another probe is mounted on the AFM head. For a comparison with the mathematical results, the identified holder dynamics was coupled with the free-free FE model of the probe to define the direct FRF at the probe tip using Eq. (18). This equation yields the direct FRF when the force is applied at the probe tip and the response is picked up at the tip. The direct FRF at the probe tip cannot be obtained experimentally, since it is hard to apply the direct excitation at the probe tip within a specific range of frequency. Using the RC method, this information for each probe can be easily obtained by combining the predefined holder dynamics and the FE model of the probe.

Based on Eq. (18), we obtained the direct dynamics at the tip of probe B, as shown in Figure 8. As a comparison, the direct FRF obtained from the FE model of the clamped-free (i.e., cantilever) beam is plotted in the same figure. It can be concluded that, at low frequencies, the probe showed similar dynamics to the clamped cantilever beam from the FE analysis and that the dynamics of holder did not have considerable effects on the cantilever dynamics. However, at higher frequencies, where the local modes of the holder setup were excited by the piezo actuator, the FE clamped beam deviated

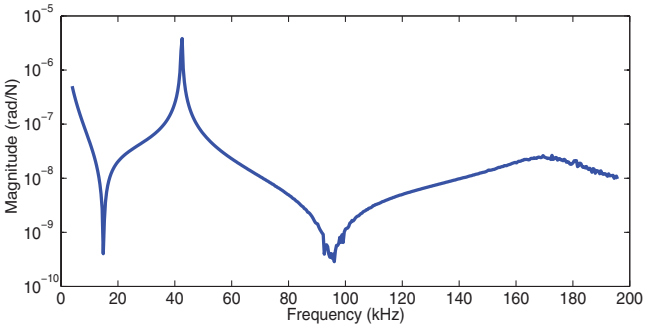


FIG. 7. (Color online) Rotational FRF at the joint ($H_{S22,fm}$).

This article is copyrighted as indicated in the article. Reuse of AIP content is subject to the terms at: http://scitationnew.aip.org/termsconditions. Downloaded to IP: 35.8.11.3 On: Mon, 25 Jan 2016 01:52:26

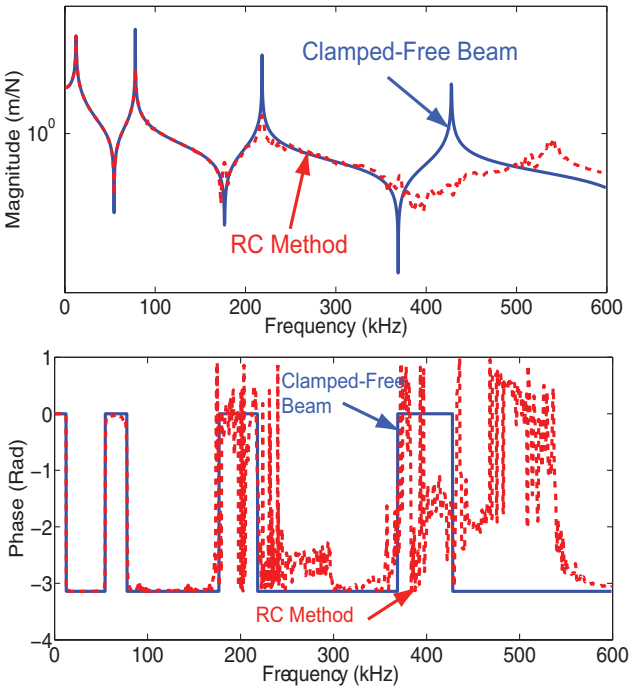


FIG. 8. (Color online) Receptance coupled vs. clamped-free FE FRF ($G_{11,ff}$) for probe B.

from the RC dynamics. As the frequency increased, the holder dynamics had considerable effects on the total dynamics of the structure and the simple clamped-free beam model could not accurately predict the actual behavior of the probe.

If the dynamics of a probe at high frequencies is of interest, the dynamics of the holder cannot be neglected. Dismissing the holder dynamics and modeling the probe as a simple clamped beam can result in deviations from the actual behavior of the probe at high frequencies, as shown in Figure 8. It is imperative to first identify the dynamics of the holder and then couple the dynamics with the mathematical model of the probe to have reliable information regarding the dynamics of the probe for a wide range of frequencies.

### B. Verifications

In order to assess the accuracy of the obtained results, two verifications were conducted. In the first verification, probe A, which was not used in extracting the holder dynamics, was studied. Using Eqs. (13) and (18), the translational FRFs ($G_{12,ff}$ and $G_{11,ff}$) for probe A were computed and compared with the FRFs obtained from the measurements. Figure 9 shows this comparison. According to this figure, the natural frequencies of the probe were predicted satisfactorily. Moreover, the magnitude of the predicted receptance showed a good correlation with the measured receptance at a wide range of frequencies. This proves that the obtained dynamics for the holder setup was reliable enough to be used in the RC method to predict both the cross and direct FRFs for a probe that was not used in the identification procedure.

For the second verification, the probe setup was completely replaced with the CSC38 probe. This probe had similar geometrical properties as probe A with a tip near the end of the probe. The dynamic properties of the holder, which were extracted from the other setup, were employed in the RC method to generate the FRF of the new probe using Eq. (13). The dynamics of the probe was obtained from the free-free FE model of the probe with a tip mass of approximately $4.03 \times 10^{-12}$ kg, which was modeled as a lumped mass and located near the end of the probe (approximately 10 $\mu$m from the end).

Figure 10 shows the comparison between the translational FRF of the CSC38 probe generated from the RC method and the FRF obtained from direct measurements on the probe when the excitation was at the base and the measurement was at the probe tip. According to this figure, the proposed method could also satisfactorily predict both the natural frequencies and the receptance curve for the probe, even after the whole probe was replaced with a new one. This implies that once we have the holder dynamics, it can be used to accurately predict the dynamics of a different setup.

One of the natural frequencies in the measured $G_{12,ff}$ was not reconstructed in the $G_{11,ff}$ curve. This may have occurred due to the fact that, by changing the location of excitation, some of the modes may not have been sufficiently excited. When the applied force was at point 2 (Figure 2), the second mode of the probe was excited and resulted in the measured FRF. However, when the excitation was at point 1 ($G_{11,ff}$), this mode may not have been excited and so did not show its influence in the reconstructed FRF.

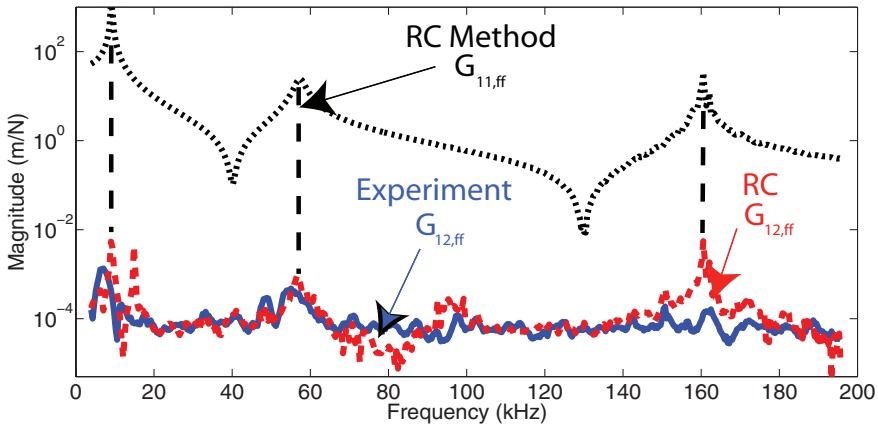


FIG. 9. (Color online) Receptance coupled FRFs ($G_{11,ff}$, $G_{12,ff}$) vs. experimental FRF ($G_{12,ff}$) for probe A.

This article is copyrighted as indicated in the article. Reuse of AIP content is subject to the terms at: http://scitationnew.aip.org/termsconditions. Downloaded to IP: 35.8.11.3 On: Mon, 25 Jan 2016 01:52:26

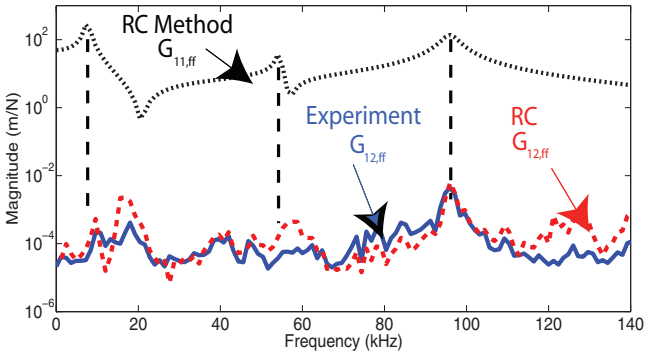


FIG. 10. (Color online) Receptance coupled FRFs ($G_{11,ff}$, $G_{12,ff}$) vs. experimental FRF ($G_{12,ff}$) for the CSC38 probe.

### C. Discussions

There were several assumptions associated with the modeling and experimental tests. The nonlinearities in the piezo actuator behavior were assumed to be negligible. This implies that the frequency content of the applied voltage to the piezo actuator excites the same frequency content of the base and probe. The noise contamination in the measurements, especially at high frequencies, may also affect the calculations. A small amount of noise can result in large deviations, particularly when the inverted matrices may be close to an ill-conditioned state.

In the FE modeling of the probes, the dimensions were chosen as provided by the vendor. However, in the microscale, there are always deviations from the actual size. Small errors in the geometry of the probes may cause inaccuracy in the results. The rotational FRF ($H_{S22,mm}$) for the holder section was also neglected. Although this assumption was verified by the FE analysis, considering this value in the formulations may result in better outcomes. In the modeling of the CSC38 probe, the tip part was modeled as a lumped mass and pointed on an arbitrary point near the end of the probe. This modeling does not accurately represent the actual mass distribution of the tip over a wide area on the probe and may cause some errors in the results.

Furthermore, the assumption of SDOF in the modal analysis, which implies that the response can be attributed to one local mode, may cause some errors in the results when there are two close modes.[19] As shown in Figures 9 and 10, there were two close modes in the FRFs near 18 kHz, which may not have complied with the local mode assumption.

In spite of these assumptions, the reconstructed receptance for the probes showed good agreement with the experimental results in a wide range of frequencies. This is important since the receptance can be employed in different applications, such as identification of the applied forces to the cutting tool during AFM probe based machining, scribing or fabrication of grooves on the surface. It is also possible to obtain complicated surface features on different samples by computing the exact required vertical and lateral forces needed at the cutting tip. Furthermore, when the linear behavior of the probe is accurately identified, it can be extended to study the dynamics of the probe in the presence of nonlinear interaction forces close to the surface of specimen.

## V. CONCLUSIONS

From the advent of AFM systems, the dynamics of the probe has received a lot of attention in the literature. The reliability of information taken from AFM scans is highly dependent on the oscillation of the cantilever at the predefined parameters, such as frequency and amplitude. To achieve the exact operating conditions and obtain reliable images, having accurate knowledge of the probe's dynamics is imperative.

The direct measurement of the receptance (i.e., displacement/force) at the probe tip is not possible, since a direct force cannot be applied at the tip due to the fragility of the probe. Moreover, a simple cantilever beam approximation for the probe does not provide the accurate dynamics, since the boundary condition of the overall AFM system is not considered. We have, therefore, proposed a modified receptance coupling method that mathematically combines the structural dynamics of the AFM system and the probe.

In this study, we investigated the receptance coupling of miniature free-free AFM probes and the holder setup system. Tipless probes were used to identify the joint dynamics between the AFM system and the probe. The most important information for an AFM operator is the behavior of probe tip in response to the interaction forces between the probe and sample. Using the proposed identification procedure for the joint dynamics and the novel receptance coupling method, it is now possible to model the direct probe dynamics at the tip.

The results were verified using a tipless probe that was not used in the joint identification. Once the holder dynamics (i.e., joint dynamics) is obtained, information can be saved in the database. This information can later be used when another probe setup, which may be different from the ones used in the identification procedure, is mounted on the AFM, in order to identify the tip dynamics without any need to repeat all the tests from the beginning. This achievement was also verified in this study by comparing the predicted dynamics of an AFM probe containing tip mass with the measured results. This probe, which had different geometry from the probes used in the identification procedure and had a tip mass near the end, was mounted on the holder setup replacing the probes used in the identification procedure.

Extracting receptance in a wide range of frequencies at the tool tip enables us to ascertain the applied forces on the tip during a surface scan or scribing process by experimentally measuring the displacement of the tip. The method can provide invaluable information on how materials behave dynamically in the nanoscale. Identification of the applied forces to the probe helps us to find tribological parameters, such as friction and adhesion, and also material distribution in composites, since they have direct relationships with the applied force. Identified forces can also be used during a scribing process on delicate materials, such as CNT polymer or biomaterials, which are hard to process and need a precise amount of force to achieve the desirable cutting dimensions. Moreover, they can be used online during a scanning process to acquire accurate phase images, which provide nanoscale information about surface structures often not revealed by other scanning probe microscopy methods.

This article is copyrighted as indicated in the article. Reuse of AIP content is subject to the terms at: http://scitationnew.aip.org/termsconditions. Downloaded to IP: 35.8.11.3 On: Mon, 25 Jan 2016 01:52:26

## ACKNOWLEDGMENTS

This work was supported by the Natural Sciences and Engineering Research Council of Canada (NSERC) and the Auto21 Network Centre of Excellence (NCE).

[1]M. Malekian, S. S. Park, D. Strathearn, Md. G. Mostofa, and M. B. G. Jun, J. Micromech. Microeng. **20**, 115016 (2010).
[2]A. P. Malshe, K. P. Rajurkar, K. R. Virwani, C. R. Taylor, D. L. Bourell, G. Levy, M. M. Sundaram, J. A. McGeough, V. Kalyanasundaram, and A. N. Samant, CIRP Ann. **59**, 628 (2010).
[3]S. I. Lee, S. W. Howell, A. Raman, and R. Reifenberger, Phys. Rev. **66**, 115409 (2002).
[4]R. Garcia and A. S. Paulo, Phys. Rev. **61**, 13381 (2000).
[5]A. S. Paulo and R. Garcia, BioPhys. J. **78**, 1599 (2000).
[6]U. Rabe, S. Amelio, E. Kester, V. Scherer, S. Hirsekorn, and W. Arnold, Ultrasonics **38**, 430 (2000).
[7]S. Rast, C. Wattinger, U. Gysin, and E. Meyer, Rev. Sci. Instrum. **71**, 2772 (2000).
[8]J. E. Sader and C. P. Green, Rev. Sci. Instrum. **75**, 878 (2004).
[9]D. A. Mendels, M. Lowe, A. Cuenat, M. G. Cain, E. Vallejo, D. Ellis, and F. Mendels, J. Micromech. Microeng. **16**, 1720 (2006).
[10]J. Melcher, S. Hu, and A. Raman, Appl. Phys. Lett. **91**, 053101 (2007).
[11]A. Salehi-Khojin, S. Bashash, and N. Jalili, J. Micromech. Microeng. **18**, 085008 (2008).
[12]R. Arinero and G. Leveque, Rev. Sci. Instrum. **74**, 104 (2003).
[13]U. Rabe, K. Janser, and W. Arnold, Rev. Sci. Instrum. **67**, 3281 (1996).
[14]S. Hu, S. Howell, A. Raman, R. Reifenberger, and M. Franchek, Trans. ASME, J. Vib. Acoust. **126**, 343 (2004).
[15]N. Sasaki, M. Tsukada, R. Tamura, K. Abe, and N. Sato, Appl. Phys. A. **66**, 287 (1998).
[16]S. S. Park, Y. Altintas, and M. Movahhedy, Int. J. Mach. Tools Manuf. **43**, 889 (2003).
[17]T. L. Schmitz, and R. R. Donalson, CIRP Ann. **49**, 303 (2000).
[18]S. N. Magonov, V. Elings, and M. H. Whangbo, J. Surf. Sci. **375**, 385 (1997).
[19]D. J. Ewins, *Modal Testing: Theory and Practice* (Research Studies, Hertfordshire, 2000).
[20]M. Tabib-Azar, K. Wong, and W. Ko, Sens. Actuators **33**, 199 (1992).
[21]T. L. Schmitz and G. S. Duncan, ASME J. Manuf. Sci. Eng. **127**, 781 (2005).
[22]S. S. Park and J. Chae, Int. J. Adv. Manuf. Technol. **35**, 1251 (2008).
[23]V. A. Spector and H. Flashner, Trans. ASME **112**, 186 (1990).
[24]S. J. Orfanidis, *Introduction to Signal Processing* (Prentice-Hall, Englewood Cliffs, NJ, 1996).

This article is copyrighted as indicated in the article. Reuse of AIP content is subject to the terms at: http://scitationnew.aip.org/termsconditions. Downloaded to IP: 35.8.11.3 On: Mon, 25 Jan 2016 01:52:26